ELSEVIER

Carbohydrate Research 337 (2002) 2023–2036

CARBOHYDRATE RESEARCH

www.elsevier.com/locate/carres

Synthesis and conformational analysis of a pentasaccharide corresponding to the cell-wall polysaccharide of the Group A *Streptococcus*

Christer Höög, Archimede Rotondo, Blair D. Johnston, B. Mario Pinto*

Department of Chemistry, Simon Fraser University, Burnaby, British Columbia, Canada V5A 1S6

Received 26 February 2002; accepted 29 May 2002

This paper is dedicated to Professor Derek Horton on the occasion of his 70th birthday

Abstract

The synthesis and conformational analysis of a pentasaccharide corresponding to a fragment of the cell-wall polysaccharide (CWPS) of the bacteria *Streptococcus* Group A are described. The polysaccharide consists of alternating α-(1→2)- and α-(1→3)-linked L-rhamnopyranose (Rha*p*) residues with branching 2-acetamido-2-deoxy-D-glucopyranose (Glc*p*NAc) residues linked β-(1→3) to alternate rhamnose rings. The pentasaccharide is of interest as a possible terminal unit on the CWPS, for use in a vaccine. The syntheses employed a trichloroacetimidate glycosyl donor. Molecular dynamics (MD) calculations of the pentasaccharide with the force fields CVFF and PARM22, both in gas phase and with explicit water present, gave different predictions for the flexibility and preferred conformational space. Metropolis Monte Carlo (MMC) calculations with the HSEA force field were also performed. Experimental data were obtained from 1D transient NOE measurements. Complete build-up curves were compared to those obtained by full relaxation matrix calculations in order to derive a model of the conformation. Overall, the best fit between experimental and calculated data was obtained with MMC simulations using the HSEA force field. Molecular dynamics and MMC simulations of a tetrasaccharide corresponding to the Group A-variant polysaccharide, which differs in structure from Group A in lacking the Glc*p*NAc residues, were also performed for purposes of comparison.

Keywords: *Streptococcus* Group A; Oligosaccharide synthesis; Conformations; NMR; Molecular dynamics simulations; Metropolis Monte Carlo calculations

1. Introduction

The β-hemolytic *Streptococcus pyogenes* or Group A (GAS) is one of the primary infective agents in humans, causing streptococcal pharyngitis (strep throat), some forms of pneumonia, toxic shock syndrome, and necrotizing fasciitis or flesh-eating disease.[1] Further complications arise because of the risk to certain individuals from the sequelae to bacterial infection such as rheumatic fever, rheumatic carditis, heart valve disease, and acute glomerulonephritis.[2–5] In addition, in the last decade, there has been an alarming increase in the incidence of streptococcal toxic shock syndrome and other invasive infections such as necrotizing fasciitis and myositis.[1b–d]

The need for culturing methods to ensure accurate diagnosis, together with the threat of antibiotic-resistant bacteria[6] in the future, make a vaccine protocol an attractive alternative to the present antibiotic protocol.[7] A vaccine strategy would also be preferred over the current therapy of invasive diseases such as streptococcal toxic shock syndrome and necrotizing fasciitis which involves high doses of antibiotics, aggressive surgery, and intravenous administration of immunoglobulins.[1b,c]

We have focused our attention on development of a carbohydrate-based vaccine based on the GAS cell-wall polysaccharide. A vaccine consisting of heat-killed,

* Corresponding author. Tel.: (604) 291-4327; fax: (604) 291-5424

E-mail address: bpinto@sfu.ca (B.M. Pinto).

0008-6215/02/$ - see front matter
PII: S0008-6215(02)00218-5

pepsin-treated bacteria has been used to immunize mice, rabbits, and humans.[8,9] The immune responses are primarily directed against the exposed carbohydrate antigens and are characterized by their restricted heterogeneity.[8] The immune response in vivo switches from IgM to IgG, indicating the action of a T cell-mediated response.[8,9]

A patent that describes the preparation of GAS polysaccharide conjugates for use as vaccines has been issued.[10] The bactericidal activity of human sera (containing antibodies to GAS polysaccharide) against several strains of GAS in vitro was demonstrated. Although this work demonstrates the viability of an approach based on a polysaccharide vaccine, the presentation of a high density of well-defined oligosaccharide epitopes in a glycoconjugate vaccine might be advantageous to elicit discriminating immune responses.[11,12]

Towards this end, we have described the synthesis of portions of the cell-wall polysaccharide that might be candidates for incorporation into vaccines. The repeating unit of the GAS cell-wall polysaccharide (CWPS) consists of a poly α-L-rhamnopyranosyl backbone composed of alternating (1→2)- and (1→3)-linkages to which *N*-acetyl-β-D-glucosamine residues are attached at the 3-position of the rhamnose residue (see Fig. 1).[13,14] We have synthesized the haptens: disaccharide (CB) **2**, linear trisaccharide (ABC) **3**, branched trisaccharide (B(C)A′) **4**, two tetrasaccharides (AB(C)A′) **5** and (B(C)A′B′) **6**, pentasaccharide (B(C)A′B′C′) **7**, and two hexasaccharides, (A(C)BA′B′C′) **8** and (B(C)A′B′(C′)A) **9** (see Fig. 1).[15–17] In addition, we have prepared glycoconjugates of **3**, **4**, **7**, and **9** for use as antigens and immunoadsorbents,[18–20] and have used the entire panel of compounds in the selection and characterization of polyclonal sera and mAbs with binding profiles for different epitopes.[18–22] Our immunochemical work[18,21,22] has indicated that the branch point and the size of the GAS antigen are crucial elements of the epitope recognized by both polyclonal and mAbs that also bind the native polysaccharide antigen.

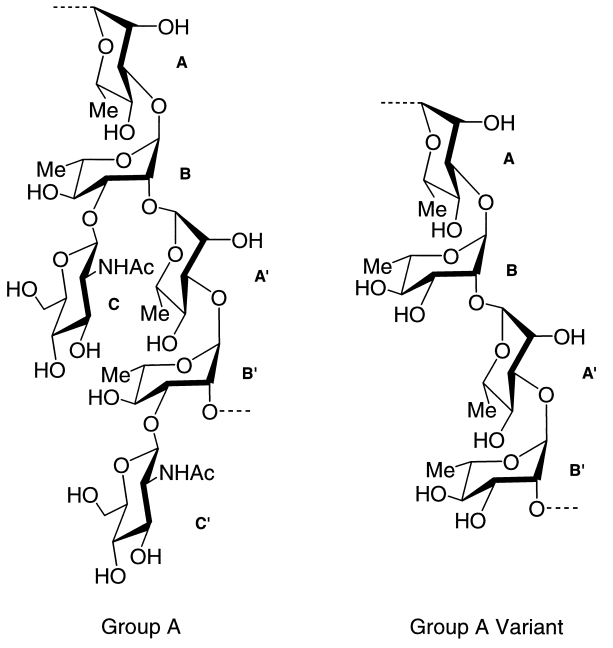

Fig. 1. Cell-wall polysaccharides of the bacteria *Streptococcus* Group A (left) and Group A-variant (right). Synthetic examples: CB, **2**; ABC, **3**; B(C)A′, **4**; AB(C)A′, **5**; B(C)A′B′, **6**; B(C)A′B′C′, **7**; A(C)BA′B′C′, **8**; B(C)A′B′(C′)A, **9**.

Conformational analysis of the oligosaccharides **4**–**9** has shown that the branch point represented in the trisaccharide **4** is a well-defined conformational feature both in the free ligand and when bound to an antibody.[23–26] The polysaccharide exists in a helix in which the rhamnosyl residues form the core of the helix and the *N*-acetylglucosamine residues are disposed on the periphery.[23,24] The helix presents the branched trisaccharide motif, as well as an accessible extended surface.[22]

We now describe the synthesis of a hitherto undescribed pentasaccharide (B(C)A′B′A) **10**, that might represent the chain terminus of the CWPS, as a suitable candidate for incorporation into a glycoconjugate vaccine. We also present its conformational analysis to gain an understanding of the possible topographies presented to the immune system.

2. Results and discussion

Synthesis.—The pentasaccharide **10** was synthesized by slight modifications of the procedures developed for the preparation of related oligosaccharides.[17] The protection strategy involved only ester protecting groups and was therefore suitable for preparation of the final oligosaccharide in the form of an allyl glycoside. We have previously found that allyl glycosides can provide a convenient tether for subsequent attachment of oligosaccharides to solid supports[20] or for conjugation to proteins.[19]

The trisaccharide acceptor **11** was prepared as previously described.[17] The required, selectively protected, rhamnopyranosyl trichloroacetimidate **12** has been recently reported[27] without characterization by NMR, which has therefore been dealt with here. Glycosylation of the acceptor **11** by donor **12**, with activation by a catalytic amount of triethylsilyl triflate, proceeded smoothly in CH_2Cl_2 to yield the tetrasaccharide **13** (Scheme 1). The sole acetate ester at the 2-position of the A′-ring was then selectively removed by methanolysis using HCl in methanol to generate the tetrasaccharide glycosyl acceptor **14**. Glycosylation with **12**, as before, afforded the required protected pentasaccha-

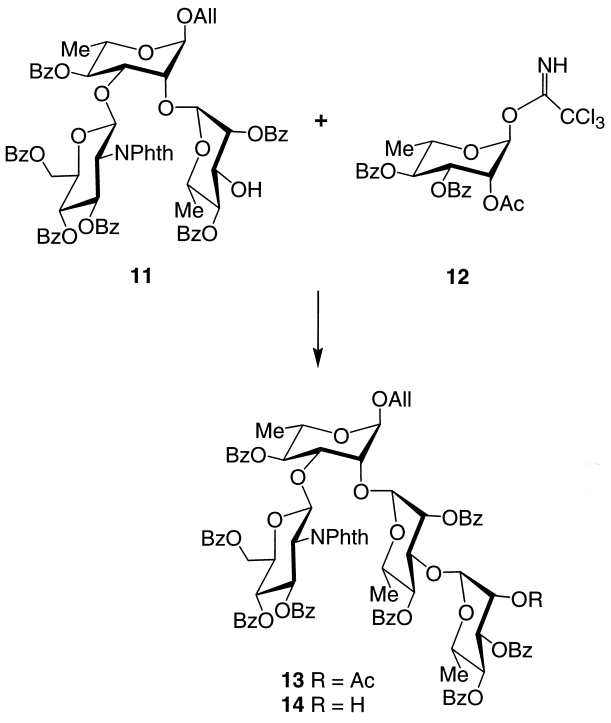

Scheme 1.

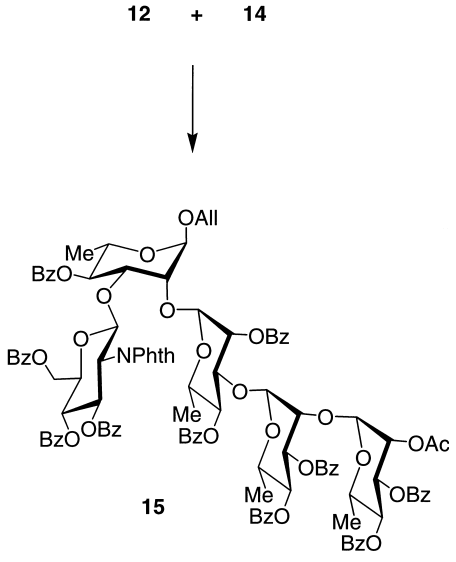

Scheme 2.

ride **15** (Scheme 2). Deprotection by successive treatment with NaOMe–MeOH and then ethylenediamine removed all of the protecting groups, and the free amine at the 2-position of ring-C was then selectively acetylated with acetic anhydride in methanol to give the crude pentasaccharide **10**. In order to facilitate purification, it proved necessary to re-acetylate all free hydroxyl groups to give the protected pentasaccharide **16**, which was more amenable to purification by chromatography on silica gel. Deprotection under Zemplén conditions regenerated the pure pentasaccharide **10** (Scheme 3).

NMR analysis.—The ^{1}H NMR spectrum of the pentasaccharide **10** exhibited a set of five downfield doublets corresponding to the five anomeric protons. One of these doublets, at δ 4.69, was unique in having the larger $J_{1,2}$ coupling constant (8.4 Hz) expected for a β-*N*-acetylglycosamine glycoside. This resonance was assigned to H-1 of the C-ring and provided a convenient starting point for assignment of the other proton resonances, particularly in the crowded region between δ 4.4 and δ 3.4. Analysis of the COSY spectrum provided complete assignment of the C-ring ^{1}H resonances. A TOCSY spectrum allowed resonances of all four rhamnose residues to be associated with their ^{1}H resonances, which appeared as four well-resolved doublets in the δ 5.2–4.8 region, each having the small $J_{1,2}$ coupling constant (1.4–1.7 Hz) characteristic of α-L-rhamnopyranosides.

Assignment of the four sets of resonances to individual rhamnose rings proceeded from analysis of NOESY, ROESY and 1D-NOE difference spectra. The 600-MHz NOESY spectrum (mixing time 250 ms) of **1** exhibited only a few, very small, negative NOE correlations. The size of pentasaccharide **1** is such that the

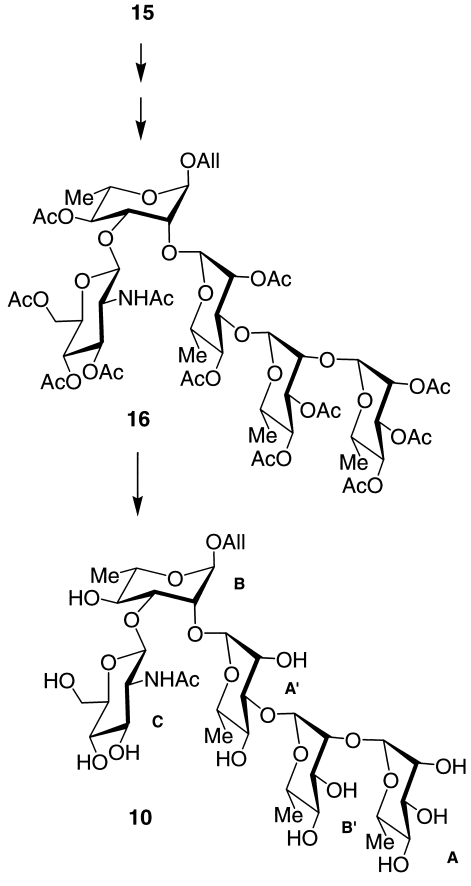

Scheme 3.

correlation times resulting from molecular tumbling result in only small NOE values. ROESY spectra (obtained with continuous spin–lock irradiation times varying between 100 and 500 ms) were similar, except that the correlations were now positive with respect to the negative diagonal peaks. Despite their low intensity, several inter-ring correlations were obvious. Two of the four rhamnose H-1 resonances exhibited cross-glycosyl NOE correlations with H-2 resonances of other rhamnose residues. These H-1 resonances were assigned to either the A′ or the A rings. One rhamnose residue showed an H-1 to H-3 cross-glycosyl NOE and was thus assigned as ring B′. The remaining rhamnose H-1 signal was correlated with the OCH_2 resonances of the allyl group and, therefore, must correspond to H-1 of the B-ring. ROESY correlations between non-anomeric resonances in the δ 4.2 to δ 3.5 region were obscured by strong TOCSY breakthrough peaks.

Differentiation of the A and A′ rhamnose resonances was achieved by 1D transient NOE difference experiments. Inversion of the H-2_B resonance with a selective Gaussian-shaped pulse showed the expected enhancements for the H-1_B and H-3_B signals and a slightly greater enhancement for a single rhamnose H-1 resonance at δ 5.17. This was assigned as H-$1_{A'}$. The remaining possibility, the rhamnose H-1 resonance at δ 4.97, showed no such enhancement, and, therefore, this resonance must be that of H-1_A. Corroborative evidence for this assignment was provided when inversion of the H-1_A resonance resulted in enhancement of the H-$2_{B'}$ signal and had no effect on the H-2_B resonance.

Since TOCSY correlations allowed the association of each rhamnose H-1 with all other proton resonances on the same ring, the ^{1}H NMR spectrum assignment was completed. The spectral dispersion was such that only the H-6_C and H-3_C resonances exhibited significant second-order effects due to overlap of H-4_C and H-5_C coupled resonances.

Analysis of the ^{13}C–^{1}H correlated spectrum then allowed complete assignment of the ^{13}C NMR spectrum. The one-bond, $J_{C1,H1}$ coupling constants of the rhamnopyranose residues were measured from a coupled ^{13}C–^{1}H correlated spectrum and varied from 173 to 178 Hz, such values being consistent with the α-configuration.[28]

Conformational analysis.—The repeating units of the cell-wall polysaccharide of *Streptococcus* Group A and variant A strain are shown in Fig. 1. The conformations of the pentasaccharide **10** and tetrasaccharide **17**, corresponding to fragments of the cell-wall polysaccharides of the *Streptococcus* Group A and variant A bacteria, respectively (see Fig. 1), were analyzed with molecular dynamics simulations employing the CVFF and CHARMM force fields. Metropolis Monte Carlo (MMC) simulations of the pentasaccharide **10** and tetrasaccharide **17** were also performed with the GEGOP program. In the case of the pentasaccharide, the calculated NOE data and corresponding ^{1}H–^{1}H distances were compared with experimental NOE data.

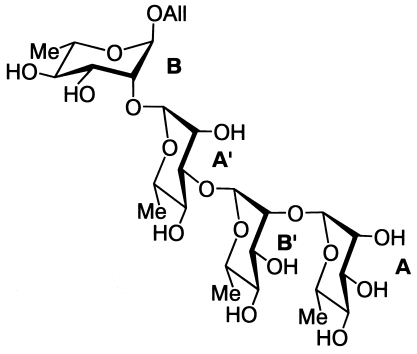

17

(a) Computations. Results from the molecular dynamics simulations of **10** are presented in scatterplots about the ϕ and ψ torsion angles. Fig. 2 indicates highly populated regions of the ϕ/ψ-space, as shown as blackened regions on the plot. The scatterplots from a 10 ns molecular dynamics simulation with the CVFF force field (simulation IV), in vacuo, is shown in Fig. 2a: two roughly equally populated states can be discerned for the non-reducing end, i.e., between residue A and B′. State **A** is characterized by an average $\phi_{A\rightarrow B'}$ torsion angle of 55° and $\psi_{A\rightarrow B'} = 11°$ for the terminal α-L-Rha*p*-(1→2)-α-L-Rha*p* linkage, whereas for state **B**, the values are 10 and −46°, respectively (Table 1).

The next linkage, between monosaccharide B′ and A′, an α-L-Rha*p*-(1→3)-α-L-Rha*p* linkage, $\phi_{B'\rightarrow A'}$ shows two different states, while $\psi_{B'\rightarrow A'}$ remains in the *−gauche* conformation. The time scales for persistence of these states are in the nanosecond region (Fig. 3). The second α-L-Rha*p*-(1→2)-α-L-Rha*p* linkage, A′→B, shows different behavior compared to that (A→B′) at the non-reducing end. There is now only one populated conformer, and it does not correspond to either state **A** or **B**. The average value for $\phi_{A'\rightarrow B}$, which shows the largest change, is −5°, while for $\psi_{A'\rightarrow B}$ it is −16°. The β-(1→3)-linkage between the *N*-acetylglucosamine (GlcNAc) and rhamnose (Rha) residues (C→B) exhibits two conformations, in which flexibility is displayed at the $\psi_{C\rightarrow B}$ torsion angle, and an energy barrier is located at −50°. Simulation V, employing a 20-ns MD simulation with the CVFF force field, shows the population of the anti conformer, $\phi_{C\rightarrow B} = \sim 180°$, during the last 2 ns and no transition back to the *+gauche* conformation is observed.

The molecular dynamics simulations employing the CHARMM-based force field (simulation I–III) give a different picture of the preferred conformations of **10** (Fig. 2b). While the molecular dynamics simulations with InsightII/Discover using the force field CVFF show two equally populated conformations at the non-reduc-

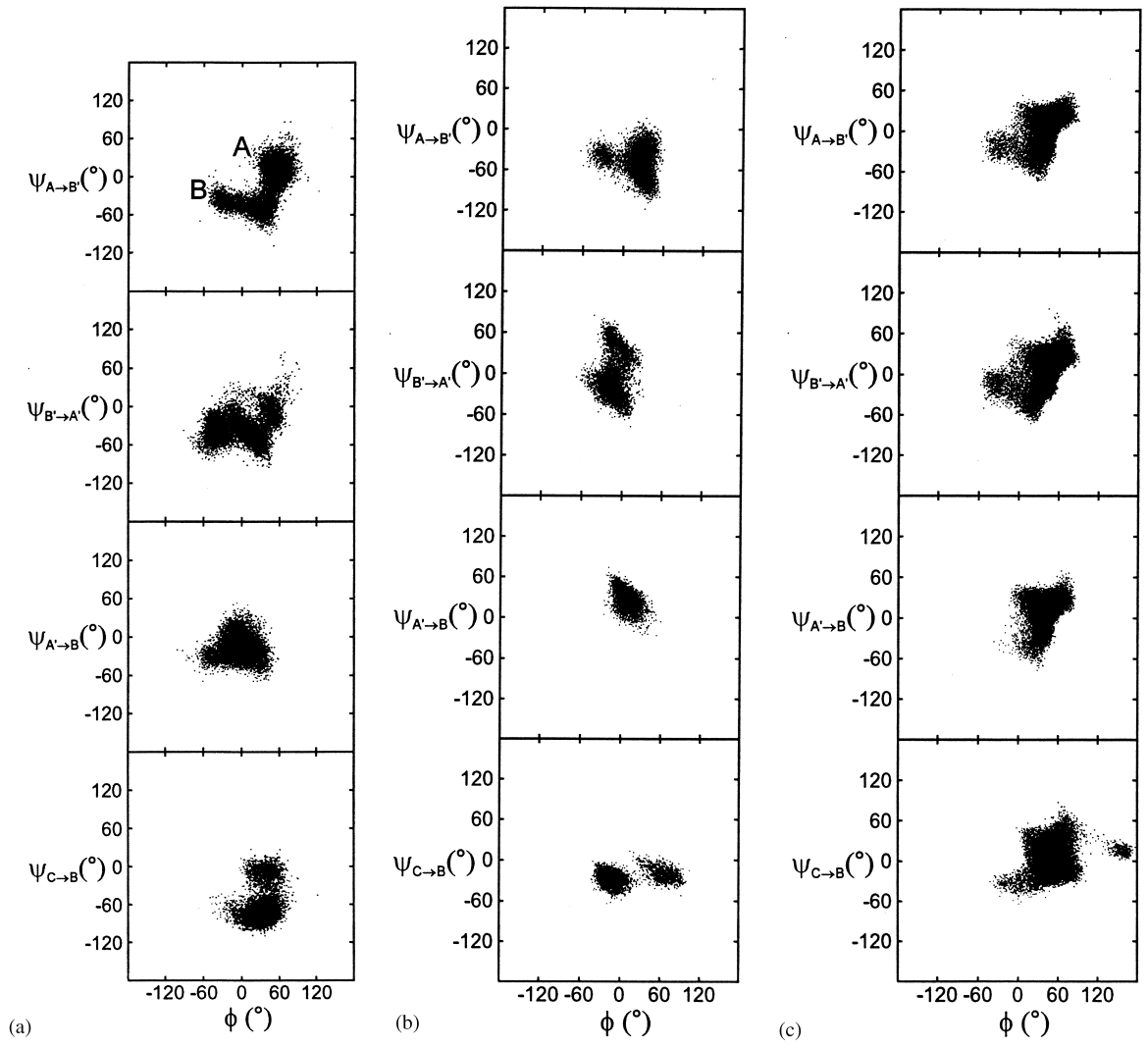

Fig. 2. Scatter plots of ϕ versus ψ for compound **10** from (a) simulation IV (CVFF), (b) simulation III (PARM22), and (c) simulation VI (HSEA). For the CVFF simulation IV, conformational states were averaged over the following time span: (**A**) 0.0-2.0 ns, (**B**) 3.0–6.0 ns.

Table 1
Average torsion angles from the molecular dynamics (MD) and Metropolis Monte Carlo (MMC) simulations for compound **10**, with the rmsd values presented in parentheses

	PARM22			CVFF				HSEA
	Sim. I	Sim. II	Sim. III	Sim. IV	Sim. V	Conf. **A**[a]	Conf **B**[a]	Sim. VI
$\phi_{A\to B'}$	20° (21°)	31° (14°)	21° (21°)	39° (28°)	45° (24°)	55° (11°)	10° (27°)	40° (19°)
$\psi_{A\to B'}$	−55° (26°)	−41° (19°)	−49° (20°)	−9° (31°)	0° (28°)	11° (16°)	−46° (12°)	2° (23°)
$\phi_{B'\to A'}$	−13° (16°)	−30° (20°)	−13° (14°)	−2° (33°)	11° (30°)	17° (21°)	−37° (14°)	41° (22°)
$\psi_{B'\to A'}$	−29° (18°)	−60° (38°)	−5° (31°)	−37° (20°)	−32° (26°)	−36° (21°)	−41° (13°)	8° (24°)
$\phi_{A'\to B}$	12° (13°)	2° (10°)	9° (11°)	−5° (21°)	–11° (25°)	−11° (18°)	8° (17°)	40° (15°)
$\psi_{A'\to B}$	13° (32°)	31° (11°)	27° (13°)	−16° (18°)	−16° (19°)	−15° (17°)	−17° (17°)	11° (20°)
$\phi_{C\to B}$	−10° (16°)	−11° (10°)	1° (32)	31° (15°)	45° (51°)	33° (16°)	27° (14°)	53° (22°)
$\psi_{C\to B}$	−34° (12°)	−32° (10°)	−26° (9°)	−66° (23°)	−15° (28°)	−23° (24°)	−37° (11°)	4° (22°)

[a] The conformational states were averaged over the following time span: (**A**) 0.0–2.0 ns, (**B**) 3.0–6.0 ns, both from simulation IV (CVFF).

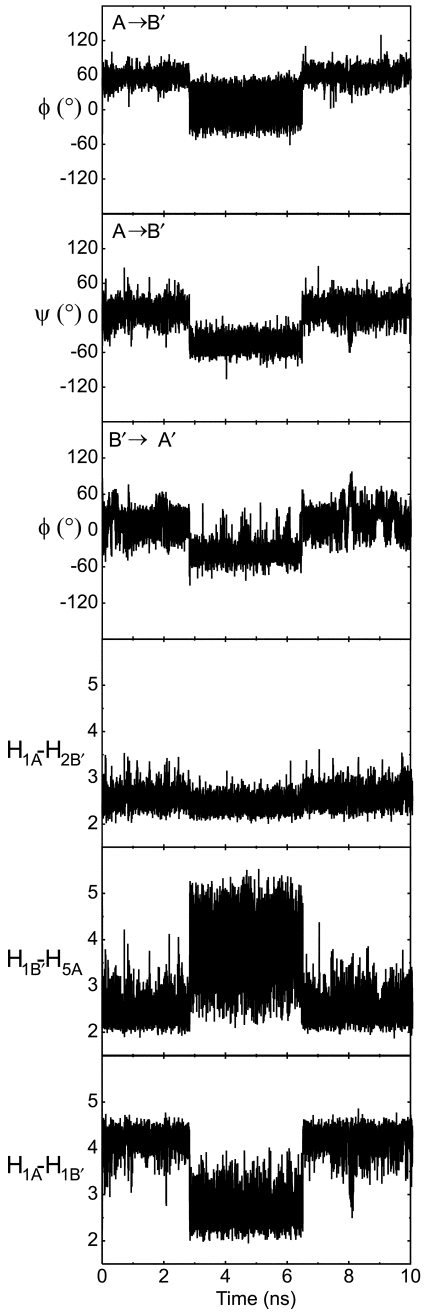

Fig. 3. Time series of torsion angles for the non-reducing end of **10** and the corresponding $^{1}H-^{1}H$ distances from simulation IV, showing the time scales for population of states **A** and **B**.

ing end ($A \rightarrow B'$), the MD simulations with PARM22 show one major and one minor populated state, together roughly corresponding to region **B**. One striking difference between the results obtained with the force fields PARM22 and CVFF is that the latter shows greater flexibility about ϕ than ψ, whereas the former shows the opposite, in agreement with the *exo*-anomeric effect.[29] Simulation I differs from simulation III in that a $-$*gauche* state is also populated for the $\psi_{A' \rightarrow B}$ linkage (Table 1). For the β-D-Glc*p*NAc-(1→3)-α-L-Rha*p* linkage, the major populated conformer shows a $\phi_{C \rightarrow B}$ $-$*gauche* angle. The torsion angle $\phi_{B' \rightarrow A'}$ shows a negative value, in contrast to the CVFF calculations where the $-$*gauche* and $+$*gauche* states are equally populated.

Table 2
Average torsion angles from the molecular dynamics (MD) and Metropolis Monte Carlo (MMC) simulations for compound **17**, with the rmsd values presented in parentheses

	PARM22	CVFF	HSEA
$\phi_{A \rightarrow B'}$	14° (25°)	41° (15°)	40° (18°)
$\psi_{A \rightarrow B'}$	−47° (20°)	−19° (24°)	2° (23°)
$\phi_{B' \rightarrow A'}$	−9° (14°)	26° (32°)	41° (21°)
$\psi_{B' \rightarrow A'}$	10° (36°)	−14° (30°)	8° (24°)
$\phi_{A' \rightarrow B}$	24° (22°)	37° (21°)	37° (20°)
$\psi_{A' \rightarrow B}$	−51° (26°)	−17° (26°)	3° (23°)

A Metropolis Monte Carlo (MMC) simulation was also performed with the HSEA force field at 600 K (simulation VI), a temperature which has previously been found to reproduce experimental $^{1}H-^{1}H$ distances well.[30] The results are illustrated in Fig. 2c and Table 2. The ϕ-torsion angles for the glycosidic linkage between two rhamnose units, i.e., $A \rightarrow B'$, $B' \rightarrow A'$ and $A' \rightarrow B$, are $\sim 40°$ and for the $C \rightarrow B$ linkage 53°. The ψ torsion angles range from 2 to 11°. The torsion angle $\phi_{C \rightarrow B}$ shows an anti conformation populated to the extent of 2% which is slightly lower than previous findings for smaller oligosaccharides.[31,32] MMC simulations with the HSEA force field have previously shown the population of an anti conformer at $\phi_{C \rightarrow B}$.[24]

Comparison of the conformations of the pentasaccharide **10** and tetrasaccharide **17** indicates that the largest difference is between the A′ and B residues, where the lack of a GlcNAc residue in the tetrasaccharide increases the available conformational space for the α-L-Rha*p*-(1→2)-α-L-Rha*p* linkage and makes the scatterplots for the $A \rightarrow B'$ and $A' \rightarrow B$ linkages more similar (Fig. 4a–c and Table 2). The MD simulation with the CVFF force field also shows that the α-L-Rha*p*-(1→3)-α-L-Rha*p* ($B' \rightarrow A'$) linkage is affected as the flexibility for $\psi_{B' \rightarrow A'}$ is increased. The conformation at the terminal non-reducing end seems to be affected only to a minor extent because of the lack of residue C. The resulting proton–proton distances from the different simulations are listed in Tables 3 and 4.

(b) Experimental. One-dimensional transient NOE spectra were measured at different mixing times, and the resulting inter-residue build-up curves are shown in Fig. 5, together with the corresponding calculated build-up curves calculated from simulation III and a combination of states **A** and **B** found in simulations IV and V. The calculated build-up curves were generated

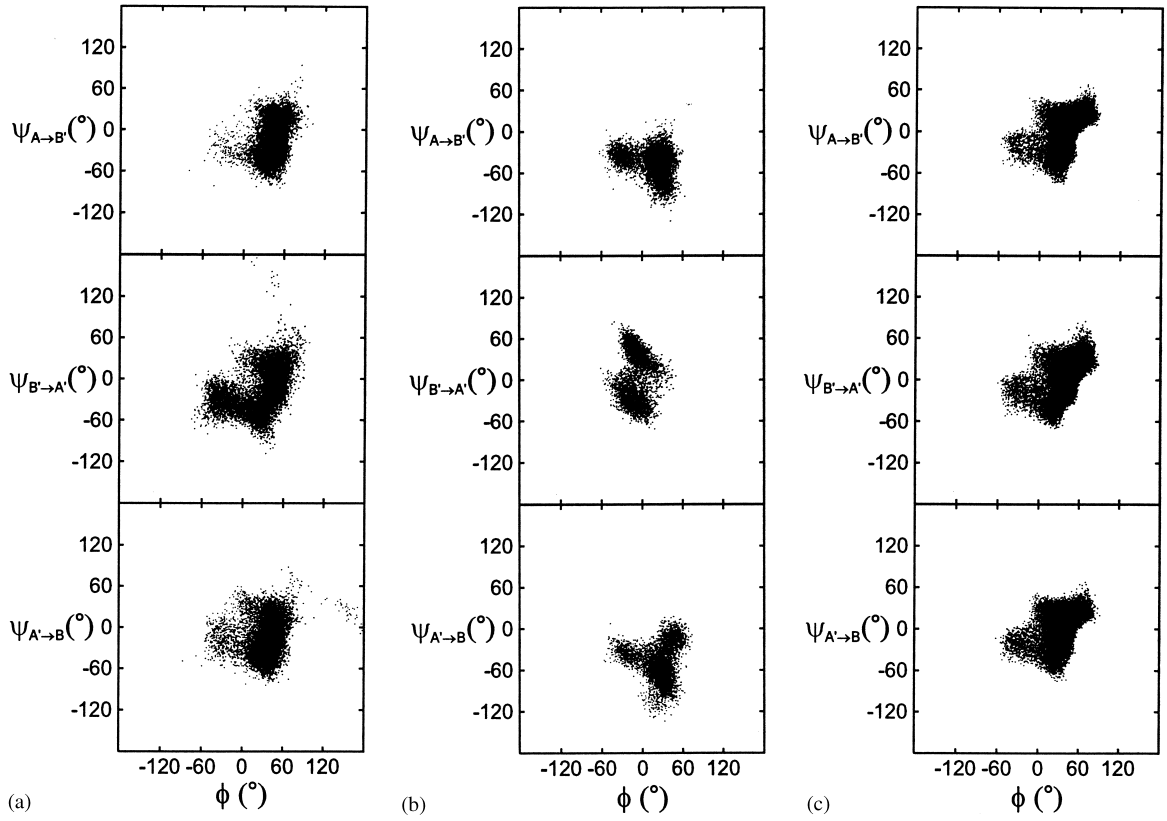

Fig. 4. Scatter plots of ϕ versus ψ for compound **17**, from simulations with the force fields (a) CVFF, (b) PARM22 and (c) HSEA.

by full relaxation matrix calculations of averaged conformations with the program CROSREL,[31] as described in our earlier publications.[23,34] The correlation time and leakage rate, R_L, obtained by fitting data for intra-residue proton pairs that have defined distances, were found to be 737 ps and 0.20 Hz, respectively, for the CVFF-generated conformations, $\mathbf{A}+\mathbf{B}$, and 596 ps and 0.0003 Hz, respectively, for the force field PARM22, with explicit water present, i.e., simulation III. The correlation times are reasonable for a pentasaccharide.[35] The agreement between calculated and the normalized experimental peak intensities is expressed by a weighted residual R_W factor, inspired by X-ray crystallography. CROSREL permits determination of the ratio of two or more conformations and the best R_W factor was reached when region **A** was populated to the extent of 82% and **B** to the extent of 18%. In general, for the non-reducing end, the combination of states **A** and **B** (■) gives the best fit to the experimental curves with the exception of the short inter-residue distances over the glycosidic linkages.

The differences in overall conformation of the pentasaccharide **10**, which is important for biological recognition, suggested by the three force fields are as follows: CVFF, in vacuo, results in a compact sphere while CHARMM, in water, and HSEA, in vacuo, give a more extended structure. This divergence is expected considering that it is well known that molecules tend to minimize their accessible surface in gas phase simulations,[36] and in the case of HSEA, the shape is due to the lack of attractive electrostatic forces. The most important torsion angles that govern the overall shape of **10** are between the central residues, i.e., the torsion angles between $B'\rightarrow A'$ and $A'\rightarrow B$. Simulation III (PARM22) and simulation IV (HSEA) give overall better fits between experimental and calculated $^1H-^1H$ distances than the combination $\mathbf{A}+\mathbf{B}$ (CVFF) (Table 4).

Table 3
Calculated[a] proton–proton distances for compound **17**

r (Å)	PARM22	CVFF	HSEA
H-1_A–H-$1_{B'}$	2.45	3.31	3.32
H-1_A–H-$2_{B'}$	2.20	2.33	2.28
H-5_A–H-$1_{B'}$	3.10	2.53	2.34
H-$1_{B'}$–H-$3_{A'}$	2.16	2.36	2.33
H-$1_{B'}$–H-$4_{A'}$	3.79	3.99	3.84
H-$1_{A'}$–H-1_B	2.42	3.26	3.32
H-$1_{A'}$–H-2_B	2.26	2.34	2.27
H-$5_{A'}$–H-1_B	2.95	2.62	2.38

[a] The calculated distances are averaged as $r=\langle r^{-6}\rangle^{-1/6}$ using the proton pair H-1–H-2 in rhamnose as the reference distance.

Table 4
Experimental and calculated[a] proton–proton distances for compound **10**

r (Å)	Exp.	CHARMM			CVFF		HSEA	**A + B**
		Sim. I	Sim. II	Sim. III	Sim. IV	Sim. V	Sim. VI	
H-1_A–H-$1_{B'}$	3.50	2.34	2.69	2.47	2.98	3.23	3.34	3.35
H-1_A–H-$2_{B'}$	2.16	2.26	2.16	2.21	2.45	2.47	2.29	2.48
H-$1_{B'}$–H-5_A	2.46	3.09	2.68	2.95	2.55	2.47	2.34	2.40
H-$1_{B'}$–H-$3_{A'}$	2.14	2.16	2.54	2.13	2.37	2.32	2.34	2.33
H-$1_{B'}$–H-$4_{A'}$	3.70	4.34	3.94	4.01	4.48	4.26	3.85	4.42
H-$1_{A'}$–H-1_B	3.84	3.16	4.02	4.00	2.91	2.83	3.57	2.89
H-$1_{A'}$–H-2_B	2.37	2.09	2.08	2.08	2.25	2.29	2.29	2.25
H-$1_{A'}$–H-1_C	4.36	2.95	2.91	3.08	4.67	4.81	4.38	3.82
H-$1_{A'}$–H-2_C	3.70	4.80	4.62	3.37	5.18	4.88	3.09	5.13
H-1_B–H-$5_{A'}$	2.52	3.24	3.42	3.36	3.59	3.65	2.41	3.68
H-1_C–H-2_B	3.25	2.56	2.65	2.81	3.14	3.29	3.64	3.17
H-1_C–H-3_B	2.27	2.21	2.20	2.19	2.30	2.37	2.39	2.30

[a] The calculated distances are averaged as $r = \langle r^{-6} \rangle^{-1/6}$ using the proton pair H-1–H-2 in rhamnose or H-1–H-3 in GlcNAc as the reference distance.

The experimental distances in Table 4 were derived by the isolated spin–pair approximation (ISPA) (Eq. (1)),[37] with the reference distance, $r_{H1,H2} = 2.52$ Å, taken from the rhamnose residues in the CHARMM simulations.

$$r_{ij} = r_{ref}(\sigma_{ref}/\sigma_{ij})^{\frac{1}{6}} \quad (1)$$

The last column in Table 4 shows the effective distances in the pentasaccharide **10** when region **A** is populated to the extent of 82% and **B** to 18%, as suggested by CROSREL. These distances are derived from the following two state relationship (Eq. (2)), where the right-hand side of the equation is given in Table 4 and x is the population of state **A**.

$$(x)\langle r^{-6}_{\text{State A}}\rangle + (1-x)\langle r^{-6}_{\text{State B}}\rangle = r^{-6}_{\mathbf{A+B}} \quad (2)$$

The distances obtained from the combined population, **A + B**, give good agreement for the terminal non-reducing end, with the exception of the inter-glycosidic distance H-1_A–H-$2_{B'}$ where both CHARMM and HSEA provide better agreement (see also the build-up curves, Fig. 5). However, PARM22, which only populates region **B**, gives the worst fit for this linkage. The experimental distances between H-1_A–H-$1_{B'}$ (3.5 Å) and H-5_A–H-$1_{B'}$ (2.46 Å) are in close agreement with values found in a conformational study of the disaccharide α-L-Rha*p*-(1→2)-α-L-Rha*p*-OMe.[38] For the central linkages, B′→A′ and A′→B′, the MMC simulation VI (HSEA) gives the best agreement with experiment; for the linkage B′→A′, simulation III (PARM22) also gives reasonable agreement. The linkage between the Glc*p*NAc and rhamnose residues is best described by the CVFF force field, with the combined conformations, **A + B**; the distances resulting from simulation VI (HSEA) also gives reasonable agreement. The calculated distance of 3.09 Å between H-$1_{A'}$–H-2_C in the MMC simulation VI of **10** is consistent with previous measurements on a corresponding hexasaccharide that has an additional Glc*p*NAc residue at the 3-position on the B′ unit.[23] For the pentasaccharide **10**, none of the force fields used gives a good fit with experimental data for the H-$1_{A'}$–H-2_C contact, although for the longer H-$1_{A'}$–H-1_C distance, the MMC simulation VI (HSEA) shows excellent agreement, whereas PARM22 and CVFF do not. The longer experimental value for H-1_A–H-2_C for **10** is difficult to explain since the other distances across the torsion angles that define the three-dimensional structure for the linkages between residue A′→B and C→B give reasonable agreement with those obtained in simulation VI. We could not obtain evidence to support the population of an *anti*-conformation at $\phi_{C\rightarrow B}$, because spectral overlap did not permit measurement of NOEs between H-2_C and H-3_B.

3. Experimental

General methods.—^{1}H NMR and ^{13}C NMR spectra were recorded with a Bruker AMX-400 or with a Bruker AMX-600 NMR spectrometer for solutions in $CDCl_3$ (internal standards, for ^{1}H: residual $CHCl_3$, δ 7.24 and for ^{13}C: $CDCl_3$, δ 77.0) or in D_2O (internal standard, for ^{1}H: HOD, δ 4.78; and for ^{13}C: MeOH, δ 49.50). First-order chemical shifts and coupling constants were obtained from one-dimensional spectra, and all assignments of proton and carbon resonances were based on COSY, NOESY, TOCSY and ^{13}C–^{1}H HMQC experiments. The α/β stereochemistry of the

glycosidic bonds was confirmed by measurement of the $^1J_{C1,H1}$ coupling constants.[28] Optical rotations were measured on a Rudolph Research Autopol II polarimeter. TLC was performed on aluminum plates precoated with Silica Gel 60 F_{254} (E. Merck) and detected with UV light and/or spraying with a solution containing 1% $Ce(SO_4)_2$ and 1.5% molybdic acid in 10% aq H_2SO_4 followed by heating. Compounds were purified by flash chromatography on Silica Gel 60 (E. Merck, 230–400 mesh). MALDI mass spectra were obtained on a PerSeptive Biosystems, Voyager DE time-of-flight spectrometer for samples dispersed in a 2,5-dihydroxybenzoic acid matrix. Microanalyses were performed by the SFU Department of Chemistry microanalytical service.

NMR spectroscopy. The pentasaccharide **10** (13 mg) was lyophilized twice from D_2O in order to exchange the hydroxyl protons; it was then redissolved in of D_2O (0.6 mL). NMR spectra were measured on a 600-MHz Bruker AMX spectrometer equipped with an inverse triple probe. Chemical shifts, referenced to external 3-trimethylsilyl-1-propanesulfonic acid (DSS), were assigned from 2D TOCSY, ROESY and HMQC experiments at 298 K. For the TOCSY spectra, 32 transients of 2048 points were accumulated for 512 t_1-increments,

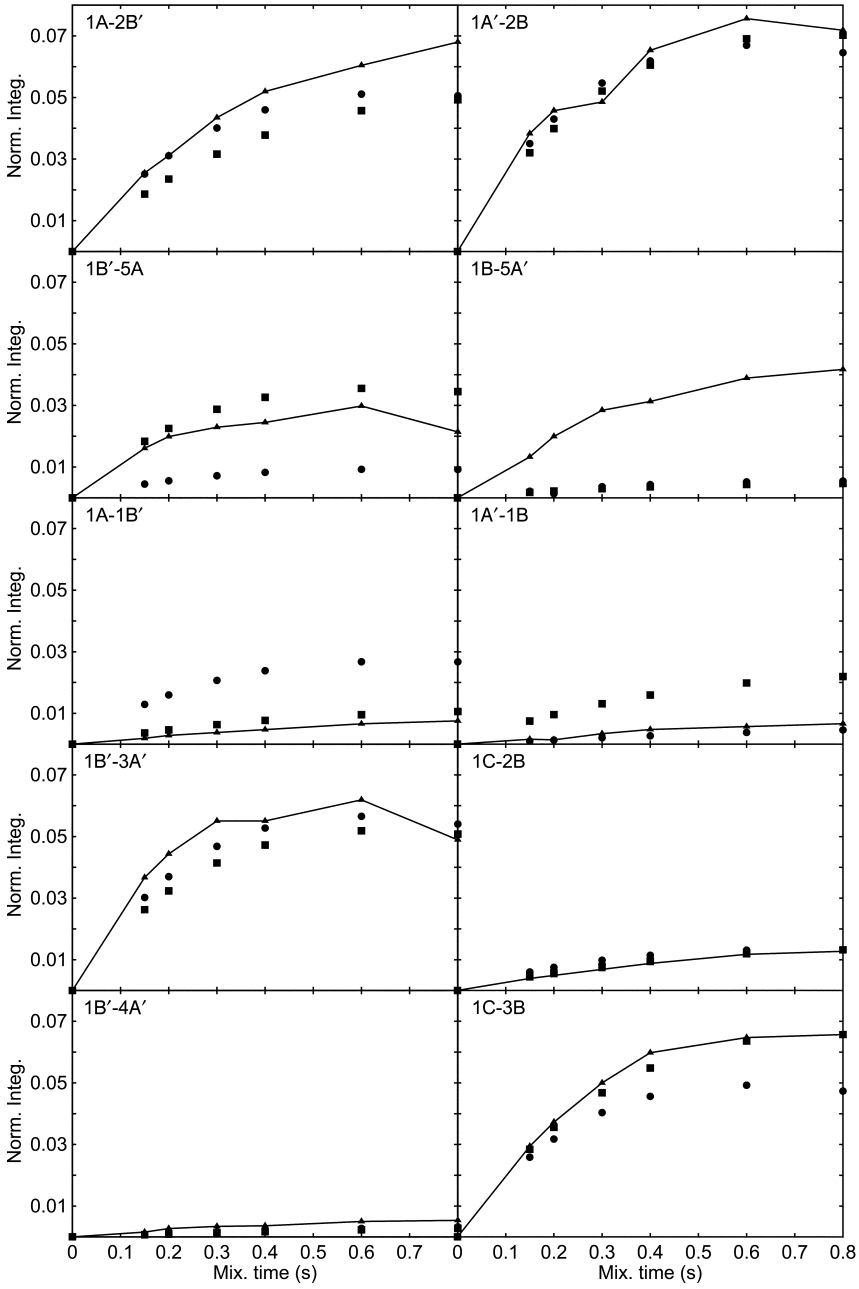

Fig. 5. Theoretical and experimental proton–proton cross-relaxation build-up curves obtained from 1D $^1H-^1H$ NOE spectra: experimental (▲), combination A + B from CVFF (■) and the average conformation from simulation III, PARM22 (●).

with the MLEV composite spin–lock pulse, and for the ROESY and HMQC experiments, 48 transients were used at every increment.

One-dimensional transient NOEs were measured at 6–8 mixing times to derive the cross-relaxation rates and thereby, proton–proton distances with the isolated spin–pair approximation (ISPA) procedure. Errors of about 5–10% in integrated intensities were estimated. Selective excitation was achieved by use of Gaussian-shaped pulses. These pulses were defined with the shape program and 1024 digital points. Seven different proton resonances were saturated with pulse durations of 80, 200, and 300 ms, and relative power attenuations were found to be 71, 78, and 81 dB, respectively.

Computer simulations. Metropolis Monte Carlo (MMC) and molecular dynamics (MD) simulations were performed for the pentasaccharide (**10**) and the tetrasaccharide (**17**). The torsion angles ϕ and ψ are defined as follows, ϕ = H-1–C-1–O-x–C-x and ψ = C-1–O-x–C-x–H-x, where x is the linkage position. For the MMC runs, the program GEGOP[39] (version 2.7), with its force field HSEA,[40] was employed. The simulations in vacuo at 600 K employed 2×10^6 macrosteps with a total acceptance ratio of 45 and 55% for **10** and **17**, respectively. The maximum step length for the glycosidic torsion angles was set to 20°.

The molecular mechanics program CHARMM,[41] version 27b4, was used for MD simulations of **10** and **17**, with explicit water present, with the CHARMM-based force field, PARM22 (Accelrys Inc., San Diego, CA, USA). The oligosaccharide was placed in a previously equilibrated cubic water box of length 34.137 Å containing 1331 TIP3P[42] water molecules, and those waters that were closer than 2.5 Å to any solute atom were removed. This procedure resulted in a system with the oligosaccharide and 1254 ± 2 (**10**) and 1274 (**17**) waters which was minimized in energy using steepest descent (250 steps) and adopted basis Newton–Raphson (250 steps) with the oligosaccharide kept fixed. After releasing the constraints, further energy minimizations were performed with steepest descent (400 steps), followed by adopted basis Newton–Raphson until the root-mean-square gradient was less than 0.01 kcal mol^{-1} Å^{-1}. Velocities were initialized at 100 K, followed by heating in 5 K increments during 8 ps to 300 K, where the system was equilibrated for 100 ps. Each simulation was run for 1 ns. Berendsens weak-coupling algorithm[43] was used to keep the temperature constant during the simulations. Minimum-image boundary conditions were used with a heuristic non-bond frequency update and a force shift cutoff[44] acting to 15 Å, using a dielectric constant of unity. SHAKE,[45] with a tolerance gradient of 10^{-4}, was used to restrain hydrogen-heavy atom bond stretch; the time step was accordingly set to 2 fs. Data were saved every 0.2 ps for analysis. All MD simulations of **10** with PARM22 had different starting conformations that were either derived from the MD simulations with the consistent valence force field (CVFF), state **A** or **B**, or with all ϕ torsion angles set to 60° and $\psi = 0°$. Simulations with the CHARMM molecular mechanics program on an SGI Octane (single processor) used a CPU time of $\sim$30 h for 100 ps.

The InsightII/Discover package was used for the molecular dynamics simulations with the force field CVFF.[46] Energy minimization with steepest descent was followed by conjugate gradient and a quasi-Newton–Raphson method (BFGS) until a maximum derivative of 0.01 kcal mol^{-1} Å^{-1} was reached. Subsequent heating and equilibration for 50 ps, with a target temperature of 298 K, were performed, followed by simulations of 10 ns (simulation IV) or 20 ns (simulation V). The time step was set to 1 fs, and no cutoffs were employed. The dielectric constant was set to r, where r is the distance between two non-bonding partially charged atoms. Coordinate sets were saved every 0.1 ps for later analysis.

Simulations I–III were performed with the PARM22 force field, with explicit water present, using the CHARMM program, simulations IV–V in the gas phase with the consistent valence force field (CVFF), and simulation VI with the HSEA force field using the program GEGOP. The simulations for the tetrasaccharide **17** are only denoted by the respective force field used.

NOE build-up curves were calculated from average conformations derived from the simulations using the CROSREL program.[33] *2-O-Acetyl-3,4-di-O-benzoyl-α-L-rhamnopyranosyl trichloroacetimidate* (**12**).—A solution of 2-*O*-acetyl-3,4-di-*O*-benzoyl-α-L-rhamnopyranose (2.70 g, 6.52 mmol)[27] in CH_2Cl_2 (50 mL) was cooled in an ice bath. Trichloroacetonitrile (2.0 mL, 20 mmol) and DBU (0.25 mL, 1.7 mmol) were added, and the mixture was stirred for 0.5 h under an N_2 atmosphere. The cooling bath was removed, and the mixture allowed to warm to rt over 15 min. Volatile material was removed by rotary evaporation and the residue was purified by column chromatography (3:2 hexanes–EtOAc) to give **4** as a pale-yellow foam (2.74 g, 75%). The ^{1}H NMR spectrum indicated that the product was >95% pure α-trichloroacetimidate, and this material was used directly in glycosylation reactions. Prolonged storage at rt resulted in partial hydrolysis. $[\alpha]_D^{22}$ +16° (*c* 1.4, CH_2Cl_2). ^{1}H NMR (400 MHz, $CDCl_3$): δ 8.80 (bs, 1 H, NH), 8.00–7.30 (m, 10 H, Ar), 6.85 (d, 1 H, $J_{1,2}$ 1.9 Hz, H-1), 5.76 (dd, 1 H, $J_{2,3}$ 3.5, $J_{3,4}$ 10.2 Hz, H-3), 5.68 (dd, 1 H, H-2), 5.65 (dd, 1 H, $J_{4,5}$ 10.1 Hz, H-4), 4.33 (dq, 1 H, H-5), 2.19 (s, 3 H, OAc), 138 (d, 3 H, $J_{5,6}$ 6.3 Hz, C*H*$_3$, H-6). ^{13}C NMR (100 MHz, $CDCl_3$): δ 169.65 (*C*=O, OAc), 165.68, 165.45 (2 × *C*=O, OBz), 160.04 (*C*=N), 133.45–128.34 (10 C, Ar), 94.75 (C-1), 70.79 (C-4),

69.49 (C-3), 68.45 (C-2), 66.73 (C-5), 20.73 (CH_3, OAc), 17.60 (CH_3, C-6).

Allyl 2-O-acetyl-3,4-di-O-benzoyl-α-L-rhamnopyranosyl-(1→3)-2,4-di-O-benzoyl-α-L-rhamnopyranosyl-(1→2)-[3,4,6-tri-O-benzoyl-2-deoxy-2-phthalimido-β-D-glucopyranosyl-(1→3)]-4-O-benzoyl-α-L-rhamnopyranoside (**13**).—A solution of the acceptor **11** (1.95 g, 1.54 mmol)[17] and the trichloroacetimidate **12** (1.04 g, 1.86 mmol) in anhyd CH_2Cl_2 (30 mL) was stirred with freshly-activated crushed 4 Å molecular sieves (2.0 g) under N_2 for 10 min at room temperature. The mixture was cooled in a −40 °C bath, and triethylsilyl triflate (30 μL, 0.13 mmol) was added. The temperature was allowed to rise to −20 °C over a period of 1 h, then the cooling bath was removed, and the mixture was allowed to warm to room temperature. Triethylamine (50 μL) was added, and the molecular sieves were removed by filtration through Celite with the aid of additional CH_2Cl_2 (100 mL). The filtrate was washed with satd $NaHCO_3$ (30 mL), dried over $MgSO_4$ and concentrated to a syrup. Flash chromatography (1:1 hexanes–EtOAc) gave the tetrasaccharide **13** (2.12 g, 83%) as a colorless, hard foam containing a trace of trichloroacetamide (^{1}H NMR, broad singlet at δ 6.6 ppm). An analytically pure sample was obtained by re-chromatography on silica gel. $[\alpha]_D^{20}$ +58° (*c* 0.76, $CHCl_3$). ^{1}H NMR (400 MHz, $CDCl_3$): δ 8.43–6.88 (m, 44 H, Ar), 6.20 (dd, 1 H, $J_{2C,3C}$ 10.5, $J_{3C,4C}$ 9.1 Hz, H-3C), 6.06 (dd, 1 H, $J_{4C,5C}$ 9.9 Hz, H-4C), 5.85–5.75 (m, 1 H, C*H*=CH$_2$), 5.75 (d, 1 H, $J_{1C,2C}$ 8.3 Hz, H-1C), 5.69 (t, 1 H, $J_{3A',4A'} = J_{4A',5A'} = 9.9$ Hz, H-4A′), 5.67 (d, 1 H, $J_{1A',2A'}$ 1.9 Hz, H-1A′), 5.65 (dd, 1 H, $J_{2A',3A'}$ 3.1 Hz, H-2A′), 5.59 (dd, 1 H, $J_{2B',3B'}$ 3.5, $J_{3B',4B'}$ 10.0 Hz, H-3B′), 5.45 (t, 1 H, $J_{3B',4B'} = J_{4B',5B'} = 9.9$ Hz, H-4B′), 5.35 (dd, 1 H, H-2C), 5.31–5.25 (m, 1 H, CH=C*H*$_2$), 5.29 (dd, 1 H, $J_{1B',2B'}$ 1.3, H-2B′), 5.21–5.17 (m, 1 H, CH=C*H*$_2$), 5.19 (d, 1 H, H-1B′), 5.17 (t, 1 H, $J_{3B,4B} = J_{4B,5B} = 9.8$ Hz, H-4B), 4.80 (d, 1 H, $J_{1B,2B}$ 1.3 Hz, H-1B), 4.71 (dd, 1 H, $J_{6C,6'C}$ 12.2, $J_{5C,6C}$ 2.6 Hz, H-6C), 4.65 (dd, 1 H, H-3A′), 4.50 (dd, 1 H, $J_{5C,6C}$ 5.6 Hz, H-6′C), 4.40 (dd, 1 H, $J_{2B,3B}$ 3.7 Hz, H-2B), 4.34 (dq, 1 H, $J_{5B',6B'}$ 6.2 Hz, H-5B′), 4.29 (ddd, 1 H, H-5C), 4.22 (dd, 1 H, H-3B), 4.17 (dq, 1 H, $J_{5A',6A'}$ 6.2 Hz, H-5A′), 4.14–4.08 (m, 1 H, OC*H*$_2$CH=CH$_2$), 3.98–3.92 (m, 1 H, OC*H*$_2$CH=CH$_2$), 3.85 (dq, 1 H, $J_{5B,6B}$ 6.2 Hz, H-5B), 1.84 (s, 3 H, C*H*$_3$, OAc), 1.33 (d, 3 H, H-6B′), 1.23 (d, 3 H, H-6A′), 1.13 (d, 3 H, H-6B); ^{13}C NMR (100 MHz, $CDCl_3$): δ 169.05 (*C*=O, OAc), 168.08 and 166.04 (2 × *C*=O, NPhth), 166.13–164.49 (8 C, 8 × *C*=O, OBz), 133.61–122.83 (55 C, Ar, *C*=CH$_2$), 117.71 (C=*C*H$_2$), 99.77 and 99.72 (C-1C and C-1A′), 99.10 (C-1B′), 98.30 (C-1B), 80.08 (C-2B), 77.53 (C-3B), 73.94 (2 C, C-4A and C-3A′), 73.33 (C-2A), 72.47 (C-4B), 72.07 (C-5C), 71.77 (C-4B′), 71.14 (C-3C), 69.74 (3 C, C-2B′, C-3B′ and C-4C), 68.14 (O*C*H$_2$C=CH$_2$), 67.59 (C-5B′), 67.04 (C-5A), 66.29 (C-5B), 62.82 (C-6C), 54.40 (C-2C), 20.43 (*C*H$_3$, OAc), 17.61, 17.55 and 17.32 (3 × *C*H$_3$, C-6A′, C-6B′, C-6B). MALDI MS Calcd for $C_{93}H_{83}NNaO_{28}$: *m*/*z* 1685.7; found *m*/*z* 1685.6. Anal. Calcd for $C_{93}H_{83}NO_{28}$: C, 67.18; H, 5.03; N, 0.84. Found: C, 67.05; H, 4.98; N, 0.86.

Allyl 3,4-di-O-benzoyl-α-L-rhamnopyranosyl-(1→3)-2,4-di-O-benzoyl-α-L-rhamnopyranosyl-(1→2)-[3,4,6-tri-O-benzoyl-2-deoxy-2-phthalimido-β-D-glucopyranosyl-(1→3)]-4-O-benzoyl-α-L-rhamnopyranoside (**14**). —A solution of HCl in MeOH was prepared by adding acetyl chloride (2.0 mL) dropwise to dry methanol (40 mL). This solution was used to dissolve the tetrasaccharide **13** (1.93 g, 1.16 mmol), and the homogeneous solution was warmed in a 40–45 °C water bath for 3.5 h. The mixture was cooled to rt and poured into a cold, stirred, satd aq $NaHCO_3$ solution (100 mL). The aqueous mixture was extracted twice with CH_2Cl_2 (100 mL, 50 mL), and the combined extracts were dried over $MgSO_4$ and evaporated to leave a colorless foam (1.57 g, 83%) that was essentially pure by NMR analysis and was used in the next reaction without purification. An analytical sample was purified by column chromatography (5:1 toluene–EtOAc) to give compound **14** as an amorphous solid. $[\alpha]_D^{20}$ +56° (*c* 0.96, $CHCl_3$). ^{1}H NMR (600 MHz, $CDCl_3$): δ 8.43–6.88 (m, 44 H, Ar), 6.24 (dd, 1 H, $J_{2C,3C}$ 10.5, $J_{3C,4C}$ 9.2 Hz, H-3C), 6.03 (dd, 1 H, $J_{4C,5C}$ 9.7 Hz, H-4C), 5.83–5.75 (m, 1 H, C*H*=CH$_2$), 5.75–5.72 (m, 2 H, H-2A′, H-1C), 5.68 (t, 1 H, $J_{3A',4A'} = J_{4A',5A'} = 9.8$ Hz, H-4A′), 5.62 (d, 1 H, $J_{1A',2A'}$ 1.6 Hz, H-1A′), 5.53 (t, 1 H, $J_{3B',4B'} = J_{4B',5B'} = 9.8$ Hz, H-4B′), 5.47 (dd, 1 H, $J_{2B',3B'}$ 3.0, $J_{3B',4B'}$ 10.1 Hz, H-3B′), 5.30 (d, 1 H, H-1B′), 5.29 (dd, 1 H, $J_{1C,2C}$ 8.1 Hz, H-2C), 5.28–5.25 (m, 1 H, CH=C*H*$_2$), 5.19–5.17 (m, 1 H, CH=C*H*$_2$), 5.17 (t, 1 H, $J_{3B,4B} = J_{4B,5B} = 10.0$ Hz, H-4B), 4.83 (d, 1 H, $J_{1B,2B}$ 1.5 Hz, H-1B), 4.71 (dd, 1 H, $J_{6C,6'C}$ 12.1, $J_{5C,6C}$ 2.7 Hz, H-6C), 4.67 (dd, 1 H, $J_{2A',3A'}$ 3.1 Hz, H-3A′), 4.55 (dd, 1 H, $J_{5C,6C}$ 5.7 Hz, H-6′C), 4.41 (dd, 1 H, $J_{2B,3B}$ 3.3 Hz, H-2B), 4.31–4.18 (m, 5 H, H-2B′, H-5B′, H-5A′, H-5C, H-3B), 4.13–4.09 (m, 1 H, OC*H*$_2$CH=CH$_2$), 3.97–3.93 (m, 1 H, OC*H*$_2$CH=CH$_2$), 3.84 (dq, 1 H, $J_{5B,6B}$ 6.3 Hz, H-5B), 1.27 (d, 3 H, $J_{5'B,6'B}$ 6.3 Hz, H-6B′), 1.25 (d, 3 H, $J_{5'A,6'A}$ 6.3 Hz, H-6A′), 1.12 (d, 3 H, H-6B); ^{13}C NMR (150 MHz, $CDCl_3$): δ 168.03 and 166.43 (2 × *C*=O, NPhth), 166.13–164.65 (8 C, 8 × *C*=O, OBz), 133.61–122.61 (55 C, Ar, *C*=CH$_2$), 117.75 (C=*C*H$_2$), 100.42 (C-1B′), 99.77 (C-1C), 99.69 (C-1A′) 98.19 (C-1B), 80.32 (C-2B), 77.60 (C-3B), 73.97 (C-3A′), 73.64 (C-4A′) 72.63 (C-2A′), 72.47 (C-4B), 72.34 (C-3B′), 72.10 (C-5C), 71.51 (C-4B′), 70.96, (C-3C), 69.79 (C-4C), 69.02 (C-2B′), 68.15 (O*C*H$_2$C=CH$_2$), 67.69 (C-5B′), 67.14 (C-5A), 66.27 (C-5B), 62.93 (C-6C), 54.40 (C-2C), 17.69, 17.46 and 17.41 (3 × *C*H$_3$, C-6A′, C-6B′, C-6B). MALDI MS Calcd for $C_{91}H_{81}NNaO_{27}$: *m*/*z* 1643.6; found *m*/*z* 1643.3. Anal. Calcd for $C_{91}H_{81}NO_{27}$: C, 67.44; H, 5.04; N, 0.86. Found: C, 67.65; H, 5.02; N, 0.74.

*Allyl 2-*O*-acetyl-3,4-di-*O*-benzoyl-α-*L*-rhamnopyranosyl-(1→2)-3,4-di-*O*-benzoyl-α-*L*-rhamnopyranosyl-(1→3)-2,4-di-*O*-benzoyl-α-*L*-rhamnopyranosyl-(1→2)-[3,4,6-tri-*O*-benzoyl-2-deoxy-2-phthalimido-β-*D*-glucopyranosyl-(1→3)]-4-*O*-benzoyl-α-*L*-rhamnopyranoside* (**15**).—Glycosylation of the tetrasaccharide **14** (1.26 g, 0.777 mmol) with the trichloroacetimidate **12** (0.522 g, 0.934 mmol) using the procedure previously described for the preparation of **13** yielded the protected pentasaccharide **15** as a colorless foam (1.38 g, 88%) after purification by column chromatography (9:1 toluene–EtOAc). $[\alpha]_D^{20}$ +63° (*c* 0.74, $CHCl_3$). ^{1}H NMR (400 MHz, $CDCl_3$): δ 8.45–6.90 (m, 54 H, Ar), 6.25 (dd, 1 H, $J_{2C,3C}$ 10.5, $J_{3C,4C}$ 9.1 Hz, H-3C), 6.02 (dd, 1 H, $J_{4C,5C}$ 10.1 Hz, H-4C), 5.85–5.75 (m, 1 H, C*H*=CH_2), 5.74 (d, 1 H, $J_{1C,2C}$ 8.1 Hz, H-1C), 5.72 (d, 1 H, H-1A′), 5.71 (dd, 1 H, $J_{2B',3B'}$ 3.6, $J_{3B',4B'}$ 10.0 Hz, H-3B′), 5.70 (dd, 1 H, $J_{3A,4A}$ 10.0 Hz, H-3A), 5.66 (dd, 1 H, $J_{1A',2A'}$ 1.6 Hz, H-2A′), 5.64 (t, 1 H, $J_{3A',4A'} = J_{4A',5A'} = 9.8$ Hz, H-4A′), 5.58 (t, 1 H, $J_{3A,4A} = J_{4A,5A} = 9.8$ Hz, H-4A), 5.50 (dd, 1 H, $J_{1A,2A}$ 2.0, $J_{2A,3A}$ 3.4 Hz, H-2A), 5.34 (dd, 1 H, H-2C), 5.34 (t, 1 H, $J_{3B',4B'} = J_{4B',5B'} = 9.7$ Hz, H-4B′), 5.33 (d, 1 H, $J_{1B',2B'}$ 1.5 Hz, H-1B′), 5.31–5.25 (m, 1 H, CH=CH_2), 5.21–5.17 (m, 1 H, CH=CH_2), 5.20 (t, 1 H, $J_{3B,4B} = J_{4B,5B} = 9.8$ Hz, H-4B), 4.80 (d, 1 H, $J_{1B,2B}$ 1.3 Hz, H-1B), 4.70 (dd, 1 H, $J_{6C,6'C}$ 12.1, $J_{5C,6C}$ 2.8 Hz, H-6C), 4.67 (dd, 1 H, $J_{2A',3A'}$ 3.0 Hz, H-3A′), 4.63 (d, 1 H, $J_{1A,2A}$ 1.8 Hz, H-1A), 4.49 (dd, 1 H, $J_{5C,6C}$ 5.5 Hz, H-6′C), 4.40 (dd, 1 H, $J_{2B,3B}$ 3.5 Hz, H-2B), 4.32 (dq, 1 H, H-5A), 4.29 (ddd, 1 H, H-5C), 4.23 (dd, 1 H, $J_{3B,4B}$ 9.7 Hz, H-3B), 4.20–4.08 (m, 3 H, 2B′, H-5A′, OCH_2CH=CH_2), 4.02 (dq, 1 H, H-5B′), 3.98–3.93 (m, 1 H, OCH_2CH=CH_2), 3.87 (dq, 1 H, H-5B), 1.97 (s, 3 H, CH_3, OAc), 1.41 (d, 3 H, $J_{5A,6A}$ 6.2 Hz, H-6A), 1.18 (d, 3 H, $J_{5A',6A'}$ 6.3 Hz, H-6A′), 1.13 (d, 3 H, $J_{5B,6B}$ 6.3 Hz, H-6B), 0.92 (d, 3 H, $J_{5B',6B'}$ 6.2 Hz, H-6B′); ^{13}C NMR (100 MHz, $CDCl_3$): δ 169.11 (*C*=O, OAc), 168.13 and 165.85 (2 × *C*=O, NPhth), 166.11–164.42 (10 C, 10 × *C*=O, OBz), 133.55–122.52 (67 C, Ar, *C*=CH_2), 117.73 (C=CH_2), 99.93 (C-1B′), 99.78 (C-1C), 99.65 (C-1A′) 98.94 (C-1A), 98.26 (C-1B), 79.61 (C-2B), 77.49 (C-3B), 76.58 (C-2B′), 74.15 (C-4A′), 73.53 (C-3A′), 73.25 (C-2A′), 72.37 (C-4B), 71.98 (C-5C), 71.94 (A-4), 71.65 (C-4B′), 71.09 (2 C, C-3A and C-3C), 69.72 (2 C, C-2A and C-4C), 69.59 (C-3B′), 68.10 (O*C*H_2C=CH_2), 67.94 (C-5A), 67.41 (C-5B′), 66.86 (C-5A′), 66.32 (C-5B), 62.81 (C-6C), 54.37 (C-2C), 20.62 (CH_3, OAc), 17.61, 17.53, 17.41 and 17.20 (4 × *C*H_3, C-6A, C-6A′, C-6B′, C-6B). MALDI MS Calcd for $C_{113}H_{101}NNaO_{34}$: *m*/*z* 2040.0; found *m*/*z* 2040.3. Anal. Calcd for $C_{113}H_{101}NO_{34}$: C, 67.29; H, 5.05; N, 0.69. Found: C, 67.31; H, 5.06; N, 0.72.

*Allyl 2,3,4-tri-*O*-acetyl-α-*L*-rhamnopyranosyl-(1→2)-3,4-di-*O*-acetyl-α-*L*-rhamnopyranosyl-(1→3)-2,4-di-*O*-acetyl-α-*L*-rhamnopyranosyl-(1→2)-[3,4,6-tri-*O*-acetyl-2-deoxy-2-acetamido-β-*D*-glucopyranosyl-(1→3)]-4-*O*-acetyl-α-*L*-rhamnopyranoside* (**16**).—The protected pentasaccharide **15** (1.20 g, 0.595 mmol) was dissolved in CH_2Cl_2 (5 mL) and MeOH (50 mL). The mixture was stirred, and a solution of 1 M NaOMe in MeOH (2.5 mL) was added. After 10 h at rt, an additional aliquot of NaOMe–MeOH solution (1 mL) was added, and the reaction was kept under N_2 for a further 36 h at rt. Trituration with hexanes (~20 mL) produced a white solid that was collected by filtration and washed thoroughly with hexanes (2 × 30 mL). The dry solid was dissolved in a mixture of EtOH (50 mL) and ethylenediamine (5 mL) and refluxed under N_2 for 24 h. The solvents were removed, and toluene (2 × 50 mL) was added and evaporated. The residue was treated with Ac_2O (5 mL) and MeOH (50 mL) for 2 h at rt and concentrated to give crude deprotected pentasaccharide **10**. Purification by flash chromatography (6:3:1 EtOAc–MeOH–H_2O) was not successful at completely removing salts and aromatic impurities as evidenced by ^{1}H NMR, so the impure product was acetylated to facilitate purification. After treatment with Ac_2O (15 mL), pyridine (15 mL) and DMAP (50 mg) for 3 h at 45 °C, the reagents were removed in vacuo, and the residue was dissolved in EtOAc (75 mL) and washed with water (30 mL), 1 M aq HCl (10 mL), satd $NaHCO_3$ solution (30 mL) and satd NaCl solution (10 mL). Purification by flash chromatography (EtOAc) gave the acetylated pentasaccharide **16** as a colorless foam (0.403 g, 51%). $[\alpha]_D^{20}$ −50° (*c* 0.88, $CHCl_3$). ^{1}H NMR (400 MHz, $CDCl_3$): δ 6.50 (br d, 1 H $J_{NH,C2}$ 6.9 Hz, N*H*Ac), 5.97 (dd, 1 H, $J_{2C,3C}$ 10.7, $J_{3C,4C}$ 9.1 Hz, H-3C), 5.94–5.83 (m, 1 H, C*H*=CH_2), 5.37 (d, 1 H, $J_{1C,2C}$ 8.1 Hz, H-1C), 5.34 (dd, 1 H, $J_{1A',2A'}$ 1.9, $J_{2A',3A'}$ 3.4 Hz, H-2A′), 5.32 (dd, 1 H, $J_{2A,3A}$ 3.4, $J_{3A,4A}$ 10.0 Hz, H-3A), 5.32–5.26 (m, 1 H, CH=CH_2), 5.26 (dd, 1 H, $J_{1A,2A}$ 1.8 Hz, H-2A), 5.23–5.19 (m, 1 H, CH=CH_2), 5.12–5.03 (m, 5 H, H-1A′, H-4A′, H-3B′, H-4B′, H-4A), 5.00 (t, 1 H, $J_{3B,4B} = J_{4B,5B} = 9.9$ Hz, H-4B), 4.97 (d, 1 H, $J_{1B',2B'}$ 1.7 Hz, H-1B′), 4.90 (dd, 1 H, $J_{4C,5C}$ 10.1 Hz, H-4C), 4.76 (d, 1 H, $J_{1A,2A}$ 1.7 Hz, H-1A), 4.72 (d, 1 H, $J_{1B,2B}$ 1.4 Hz, H-1B), 4.23 (dd, 1 H, $J_{6C,6'C}$ 12.2, $J_{5C,6C}$ 4.6 Hz, H-6C), 4.19 (dd, 1 H, $J_{2A',3A'}$ 3.4, $J_{3A',4A'}$ 9.9 Hz, H-3A′), 4.17–4.13 (m, 1 H, OCH_2CH=CH_2), 4.14 (dd, 1 H, $J_{3B,4B}$ 9.7 H-3B), 4.07 (dd, 1 H, $J_{5C,6C}$ 2.5 Hz, H-6′C), 4.02 (dq, 1 H, H-5B′), 4.01–3.95 (m, 1 H, OCH_2CH=CH_2), 4.00 (dd, 1 H, $J_{2B,3B}$ 3.3 Hz, H-2B), 3.91 (dd, 1 H H-2B), 3.89 (dq, 1 H, H-5A′), 3.83 (m, 1 H H-5A), 3.76 (ddd, 1 H, H-5C), 3.73 (dq, 1 H, H-5B), 2.74 (ddd, 1 H, H-2C), 2.25–1.87 (12 s, 36 H, 12 × CH_3, 12 OAc), 1.24 (d, 3 H, $J_{5A,6A}$ 6.1 Hz, H-6A), 1.22 (d, 3 H, $J_{5B',6B'}$ 6.5 Hz, H-6B′), 1.17 (d, 3 H, $J_{5A',6A'}$ 6.5 Hz, H-6A′), 1.15 (d, 3 H, $J_{5B,6B}$ 6.4 Hz, H-6B); ^{13}C NMR (100 MHz, $CDCl_3$): δ 171.61–169.50 (12 C, 12 × *C*=O, NHAc and 11 × OAc), 133.51 (*C*=CH_2), 117.70 (C=CH_2), 99.56 (2 C, C-1A and C-1B′), 99.24 (C-1A′), 98.36 (C-1C), 98.13 (C-1B), 78.40 (C-2B),

77.48 (C-2B′), 74.32 (C-3B), 73.25 (C-3A′), 72.84 (C-4), 72.51 (C-4B), 71.42 (2 C, C-2A′ and C-5C), 71.04 (C-4), 70.89 (C-4), 70.21 (C-3B′), 70.07, (C-3C), 69.90 (2 C, C-2A, C-4C), 68.59 (C-3A), 68.01 ($OCH_2C{=}CH_2$), 67.60 (C-5A), 67.20 (C-5B′), 67.00 (C-5A′), 66.49 (C-5B), 62.38 (C-6C), 57.75 (C-2C), 23.14–20.70 (12 C, $12 \times CH_3$, NHAc and $11 \times$ OAc), 17.51, 17.38 (2 C), and 17.30 ($4 \times CH_3$, C-6A, C-6A′, C-6B′, C-6B). MALDI MS Calcd for $C_{57}H_{81}NO_{33}$: m/z 1330.5; found m/z 1330.9. Anal. Calcd for $C_{57}H_{81}NNaO_{33}$: C, 52.33; H, 6.24; N, 1.07. Found: C, 52.60; H, 6.19; N, 1.00.

Allyl α-L-rhamnopyranosyl-(1→2)-α-L-rhamnopyranosyl-(1→3)-α-L-rhamnopyranosyl-(1→2)-[2-deoxy-2-acetamido-β-D-glucopyranosyl-(1→3)]-α-L-rhamnopyranoside (**10**).—The acetylated pentasaccharide **16** (0.322 g, 0.246 mmol) was dissolved in dry MeOH (20 mL) and placed under N_2. A 1.0 M solution of NaOMe in MeOH (1.0 mL) was added, and the mixture was kept at rt for 3.5 h. A second aliquot of the NaOMe–MeOH solution (1.0 mL) was then added, and the reaction was allowed to continue for a further 2 h. The base was neutralized by the addition of an excess of Rexyn 101 (H^+) resin, and the mixture was filtered and concentrated to a syrupy residue that was purified by flash chromatography (6:3:1 EtOAc–MeOH–H_2O) to give a colorless solid. The solid was dissolved in water (4 mL) and freeze-dried to give the pentasaccharide **10** (0.188 g, 88%) as a fluffy amorphous solid. $[\alpha]_D^{20}$ −76° (*c* 0.82, MeOH). ^{1}H NMR (600 MHz, D_2O): δ 6.00–5.93 (m, 1 H, C*H*=CH_2), 5.39–5.35 (m, 1 H, CH=CH_2), 5.33–5.30 (m, 1 H, CH=CH_2), 5.20 (d, 1 H, $J_{1B',2B'}$ 1.4 Hz, H-1B′), 5.18 (d, 1 H, $J_{1A',2A'}$ 1.7 Hz, H-1A′), 4.97 (d, 1 H, $J_{1A,2A}$ 1.7 Hz, H-1A), 4.87 (d, 1 H, $J_{1B,2B}$ 1.7 Hz, H-1B), 4.69 (d, 1 H, $J_{1C,2C}$ 8.4 Hz, H-1C), 4.26–4.22 (m, 1 H, OCH_2CH=CH_2), 4.18 (dd, 1 H, $J_{2B,3B}$ 3.0 Hz, H-2B), 4.11–4.07 (m, 1 H, OCH_2CH=CH_2), 4.09 ($2 \times$ dd, 2 H, $J_{2A,3A}$ 3.4, $J_{2A',3A'}$ 3.2 Hz, H-2A and H-2A′), 4.07 (dd, 1 H, $J_{2B',3B'}$ 3.4 Hz, H-2B′), 3.96 (dd, 1 H, $J_{3B',4B'}$ 9.9 Hz, H-3B′), 3.95–3.91 (2nd order m, 1 H, H-6C), 3.87 (dd, 1 H, $J_{3B,4B}$ 9.8 Hz, H-3B), 3.84 (dd, 1 H, $J_{3B',4B'}$ 9.9 Hz, H-3A′), 3.82 (dq, 1 H, H-5B′), 3.81 (dd, 1 H, $J_{3A,4A}$ 9.8 Hz, H-3A), 3.79–3.75 (2nd order m, 1 H, H-6′C), 3.74 (dq, 1 H, H-5B), 3.73 (dd, 1 H, $J_{2C,3C}$ 10.2, H-2C), 3.73 (dq, 1 H, H-5A′), 3.71 (dq, 1 H, H-5A), 3.58 (dd, 1 H, $J_{4A',5A'}$ 9.7 Hz, H-4A′), 3.57–3.52 (2nd order m, 1 H, H-3C), 3.52 (dd, 1 H, $J_{4B,5B}$ 9.7 Hz, H-4B), 3.50 (dd, 1 H, $J_{4B',5B'}$ 9.8 Hz, H-4B′), 3.48–3.44 (2nd order m, 2 H, H-4C and H-5C), 3.45 (dd, 1 H, $J_{4A,5A}$ 9.8 Hz, H-4A), 2.03 (s, 3 H, CH_3, NHOAc), 1.33 (d, 3 H, $J_{5B',6B'}$ 6.3 Hz, 6B′-CH_3), 1.30 (d, 3 H, $J_{5B,6B}$ 6.2 Hz, 6B-CH_3), 1.28 (d, 3 H, $J_{5A',6A'}$ 6.3 Hz, 6A′-CH_3), 1.27 (d, 3 H, $J_{5A,6A}$ 6.2 Hz, 6A-CH_3); ^{13}C NMR (100 MHz, D_2O): δ 175.09 (*C*=O, NHAc), 133.68 (*C*=CH_2), 119.37 (C=CH_2), 103.22 ($^1J_{C-H}$ 159 Hz, C-1C), 102.93 ($^1J_{C-H}$ 173 Hz, C-1A), 101.99 ($^1J_{C-H}$ 173 Hz, C-1A′), 101.31 ($^1J_{C-H}$ 178 Hz, C-1B′), 98.17 (C-1B), 80.56 (C-3B), 78.70 (C-2B′), 77.25 (C-2B), 77.19 (C-3A′), 76.40 (C-5C), 74.51 (C-3C), 72.76 (C-4B′), 72.63 (C-4A), 72.37 (C-4A′), 71.86 (C-4B), 70.69 (C-3A), 70.64 (C-3B′), 70.58 (C-2A), 70.41 (2 C, C-2A′ and C-4C), 69.91 (C-5B), 69.73 (3 C, C-5A, C-5B′ and C-5A′), 68.82 ($OCH_2C{=}CH_2$), 61.43 (C-6C), 56.49 (C-2C), 17.44, 17.23 (2 C), 17.14 (4 C, $4 \times CH_3$, C-6A, C-6A′, C-6B′, C-6B). MALDI MS Calcd for $C_{35}H_{59}NNaO_{22}$: m/z 868.8; found m/z 868.5. Anal. Calcd for $C_{35}H_{59}NO_{22}$: C, 49.70; H, 7.03; N, 1.66. Found: C, 49.40; H, 7.28; N, 1.65.

4. Conclusions

The efficient synthesis of a pentasaccharide **10**, corresponding to a portion of the cell-wall polysaccharide of the Group A *Streptococcus*, has been accomplished. A sufficient number of experimental inter-glycosidic NOE contacts for every linkage in the pentasaccharide **10** made the determination of its conformation possible. The pentasaccharide **10** was found to populate one major conformation with an overall extended shape. The conformation calculated by MMC simulations with the HSEA force field showed the best fit with experimental NOE data, as in previous investigations of the conformations of oligosaccharides.[47] It can also be concluded that the CVFF force field gives better agreement with experiment at the terminal residues, whereas the CHARMM-based force field, PARM22, gives more satisfactory results for the more rigid, central part of the molecule.

Acknowledgements

We are grateful to the Natural Sciences and Engineering Research Council of Canada for financial support of this work and the Wenner–Gren Foundation, Sweden, for a postdoctoral fellowship (to C.H.).

References

1. (a) *Streptococcal Diseases and the Immune Response*; Read, S. E.; Zabriskie, J. B., Eds.; Academic Press: New York, 1980;
   (b) Weiss, K. A.; Laverdiere, M. *Can. J. Surg.* **1997**, *40*, 18–25;
   (c) Stevens, D. L. *Immunol. Invest.* **1997**, *26*, 129–150;
   (d) Nowak, R. *Science* **1994**, *264*, 1665.
2. Bisno, A. L. Nonsuppurative Poststreptococcal Sequelae: Rheumatic Fever and Glomerulonephritis. In *Principles and Practice of Infectious Diseases*; Mandell, G. L.; Douglas, R. G.; Bennett, J. E., Eds., 2nd ed.; Wiley: New York, 1985; pp 1133–1142.
3. (a) World Health Organization: Community Control of Rheumatic Heart Disease in Developing Countries. 1. A Major Public Health Problem, *WHO Chronicle*, **1980**, *34*, 336–345;

(b) Markowitz, M. *Clin. Therapeutics* **1981**, *4*, 240–251.
4. Wannamaker, L. W. *Rev. Infect. Dis.* **1979**, *1*, 967–975.
5. Zabriskie, J. B. *Circulation* **1985**, *71*, 1077–1086.
6. Wright, K. *Science* **1990**, *249*, 22–24.
7. Rotta, J. Streptococci: Prospects for Vaccines. In *Towards Better Carbohydrate Vaccines*; Bell, R.; Torrigiani, G., Eds.; John Wiley & Sons: New York, 1987; pp 203–218.
8. Braun, D. G.; Schalch, W.; Schmid, I. The Restricted Antibody Response to Streptococcal Group Antigens in Animals and Man: A Complex Trait. In *Streptococcal Diseases and the Immune Response*; Read, S. E.; Zabriskie, J. B., Eds.; Academic Press: New York, 1980; pp 317–333.
9. Emmrich, F.; Schilling, B.; Eichmann, K. *J. Exp. Med* **1985**, *161*, 547–562.
10. Blake, M. S.; Zabriskie, J. B.; Tai, J. Y.; Michon, F. *US Patent* 5,866,135 (**1999**).
11. Benaissa-Trouw, B.; Lefeber, D. J.; Kamerling, J. P.; Vliegenthart, J. F. G.; Kraaijeveld, K.; Snippe, H. *Infect. Immun.* **2001**, *69*, 4698–4701.
12. Pozsgay, V. *Adv. Chem. Biochem.* **2001**, *56*, 153–199.
13. Coligan, J. E.; Kindt, T. J.; Krause, R. M. *Immunochemistry* **1978**, *15*, 755–760.
14. Huang, D. H.; Krishna, N. R.; Pritchard, D. G. *Carbohydr. Res.* **1986**, *155*, 193–199.
15. Pinto, B. M. *ACS Symp. Ser.* **1992**, *519*, 111–131.
16. Marino-Albernas, J.-R.; Harris, S. L.; Varma, V.; Pinto, B. M. *Carbohydr. Res.* **1993**, *245*, 245–257.
17. Auzanneau, F.-I.; Forooghian, F.; Pinto, B. M. *Carbohydr. Res.* **1996**, *291*, 21–41.
18. Reimer, K. B.; Gidney, M. A. J.; Bundle, D. R.; Pinto, B. M. *Carbohydr. Res.* **1992**, *232*, 131–142.
19. Auzanneau, F.-I.; Pinto, B. M. *Bioorg. Med. Chem.* **1996**, *4*, 2003–2010.
20. Auzanneau, F.-I.; Christensen, M. K.; Harris, S. L.; Meldal, M.; Pinto, B. M. *Can. J. Chem.* **1998**, *76*, 1109–1118.
21. Harris, S. L.; Craig, L.; Mehroke, J. S.; Rashed, M.; Zwick, M. B.; Kenar, K.; Toone, E. J.; Greenspan, N.; Auzanneau, F.-I.; Marino-Albernas, J.-R.; Pinto, B. M.; Scott, J. K. *Proc. Natl. Acad. Sci. USA* **1997**, *94*, 2454–2459.
22. Pitner, J. B.; Beyer, W. F.; Venetta, T. M.; Nycz, C.; Mitchell, M. J.; Harris, S. L.; Marino-Albernas, J.-R.; Auzanneau, F.-I.; Forooghian, F.; Pinto, B. M. *Carbohydr. Res.* **2000**, *324*, 17–29.
23. Kreis, U. C.; Varma, V.; Pinto, B. M. *Int. J. Biol. Macromol.* **1995**, *17*, 117–130.
24. Stuike-Prill, R.; Pinto, B. M. *Carbohydr. Res.* **1995**, *279*, 59–73.
25. Peters, T.; Pinto, B. M. *Curr. Opin. Struct. Biol.* **1996**, *6*, 710–720.
26. Weimar, T.; Harris, S. L.; Pitner, J. B.; Bock, K.; Pinto, B. M. *Biochemistry* **1995**, *34*, 13672–13681.
27. Wang, W.; Kong, F. *J. Carbohydr. Chem.* **1999**, *18*, 263–273.
28. Bock, K.; Pedersen, C. *J. Chem. Soc., Perkin Trans. 2* **1974**, 293–297.
29. Lemieux, R. U.; Koto, S. *Tetrahedron* **1974**, *30*, 1933–1944.
30. Peters, T.; Meyer, B.; Stuike-Prill, R.; Somorjai, R.; Brisson, J.-R. *Carbohydr. Res.* **1993**, *238*, 49–73.
31. Bukowski, R.; Morris, L. M.; Woods, R. J.; Weimar, T. *Eur. J. Org. Chem.* **2001**, 2697–2705.
32. Höög, C.; Landersjö, C.; Widmalm, G. *Chem. Eur. J.* **2001**, *7*, 3069–3076.
33. Leeflang, B. R.; Kroon-Batenburg, L. M. J. *J. Biomol. NMR* **1992**, *2*, 495–518.
34. Diaz-Quijada, G. A.; Weinberg, N.; Holdcroft, S.; Pinto, B. M. *J. Phys. Chem. A* **2002**, *106*, 1277–1285.
35. Rundlöf, T.; Venable, R. M.; Pastor, R. W.; Kowalewski, J.; Widmalm, G. *J. Am. Chem. Soc.* **1999**, *121*, 11847–11854.
36. Brooks, C. L., III; Karplus, M.; Pettitt, B. M. *Advances in Chemical Physics*, *Vol.* 71: *Proteins*: *A Theoretical Perspective of Dynamics*, *Structure and Thermodynamics*; John Wiley & Sons: New York, 1988.
37. Keepers, J. W.; James, T. L. *J. Magn. Reson.* **1984**, *57*, 404–426.
38. Widmalm, G.; Byrd, R. A.; Egan, W. *Carbohydr. Res.* **1992**, *229*, 195–211.
39. Stuike-Prill, R.; Meyer, B. *Eur. J. Biochem.* **1990**, *194*, 903–919.
40. Thøgersen, H.; Lemieux, R. U.; Bock, K.; Meyer, B. *Can. J. Chem.* **1982**, *60*, 44–57.
41. Brooks, B. R.; Bruccoleri, R. E.; Olafson, B. D.; States, D. J.; Swaminathan, S.; Karplus, M. *J. Comput. Chem.* **1983**, *4*, 187–217.
42. Jorgensen, W. L.; Chandrasekhar, J.; Madura, J. D.; Impey, R. W.; Klein, M. L. *J. Chem. Phys.* **1983**, *79*, 926–935.
43. Berendsen, H. J. C.; Postma, J. P. M.; van Gunsteren, W. F.; DiNola, A.; Haak, J. R. *J. Chem. Phys.* **1984**, *81*, 3684–3690.
44. Steinbach, P. J.; Brooks, B. R. *J. Comput. Chem.* **1994**, *15*, 667–683.
45. van Gunsteren, W. F.; Berendsen, H. J. C. *Mol. Phys.* **1977**, *34*, 1311–1327.
46. Dauber-Osguthorpe, P.; Roberts, V. A.; Osguthorpe, D. J.; Wolff, J.; Genest, M.; Hagler, A. T. *Proteins: Structure Function and Genetics* **1988**, *4*, 31–47.
47. Höög, C.; Widmalm, G. *Arch. Biochem. Biophys.* **2000**, *377*, 163–170.